Electronic Supplementary Material (ESI) for Journal of Materials Chemistry A.
This journal is © The Royal Society of Chemistry 2022

Supplementary Information

A La and Nb co-doped $BaTiO_3$ film with positive-temperature-coefficient of resistance for thermal protection of batteries

Min Zhang,[a] Sacha Fop,[ab] Denis Kramer,[cde] Nuria Garcia-Araez*[af] and Andrew L. Hector*[a]

[a]*School of Chemistry, University of Southampton, Highfield, Southampton SO17 1BJ, UK*

E-mail: N.Garcia-Araez@soton.ac.uk; A.L.Hector@soton.ac.uk

[b]*ISIS Facility, Rutherford Appleton Laboratory, Harwell OX11 0QX, UK*

[c]*Faculty of Mechanical Engineering, Helmut-Schmidt University, Holstenhofweg 85, 22043 Hamburg, Germany*

[d]*School of Engineering, University of Southampton, Highfield, Southampton SO17 1BJ, UK*

[e]*Helmholtz Zentrum HEREON, Department of Heterogeneous Catalysis, Max-Planck-Strasse 1, 21502 Geesthacht*

[f]*The Faraday Institution, Quad One, Harwell Campus, Didcot OX11 0RA, UK*

Table S1 Comparison of mechanical properties of $BaTiO_3$ and typical polymer materials used in lithium-ion batteries.

Material	Young's modulus	Ref.
$BaTiO_3$*	160 GPa	[1, 2]
Battery polymer binders wetted in electrolyte	<0.5 GPa	[3]
Battery separators wetted in electrolyte	<0.3 GPa	[4]

*Unlike polymer materials, $BaTiO_3$ is insoluble and does not swell in battery electrolytes.

Table S2 Comparison of chemical stability properties of $BaTiO_3$ and typical polymer materials used in lithium-ion batteries.

Material	Chemical stability	Ref.
$BaTiO_3$	Inert, chemically stable and non-cytotoxic. Melting point: 1625 °C	[5-7]
Polyvinylidene fluoride	Decompose at >500 °C, producing HF	[8]
Polyethylene and polypropylene	Decompose at >350 °C, producing toxic compounds	[9]

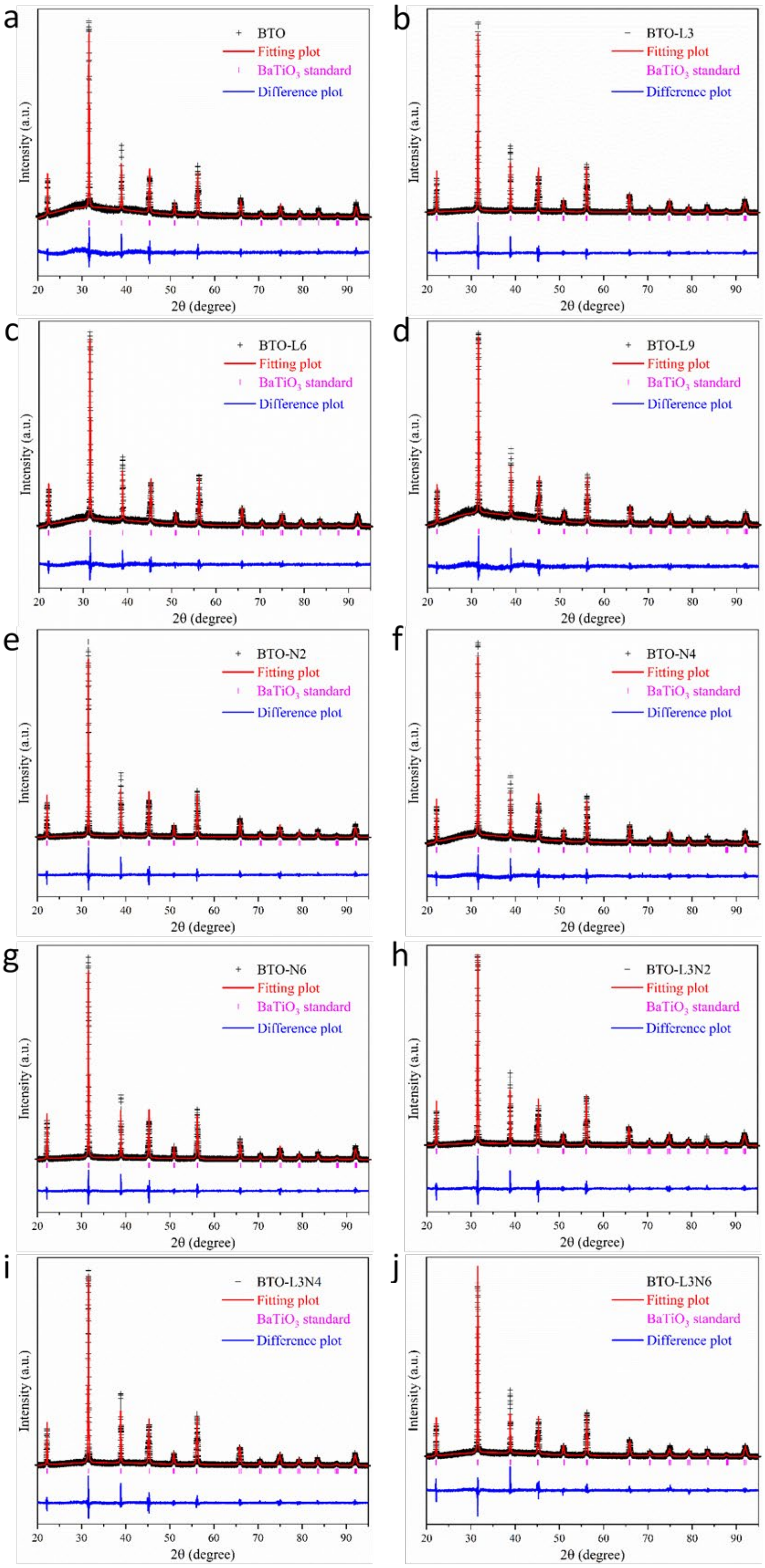

Fig. S1 Rietveld fits to the XRD patterns of a. BTO, b. BTO-L3, c. BTO-L6, d. BTO-L9, e. BTO-N2, f. BTO-N4, g. BTO-N6, h. BTO-L3N2, i. BTO-L3N4, j. BTO-L3N6 samples (sample labels explained in Table 1). The data points and Rietveld fits were overlaid as black crosses and red lines, respectively. The difference plots were shown in blue. The pink marks showed allowed reflection positions for tetragonal $BaTiO_3$ structure with space group *P4mm*.

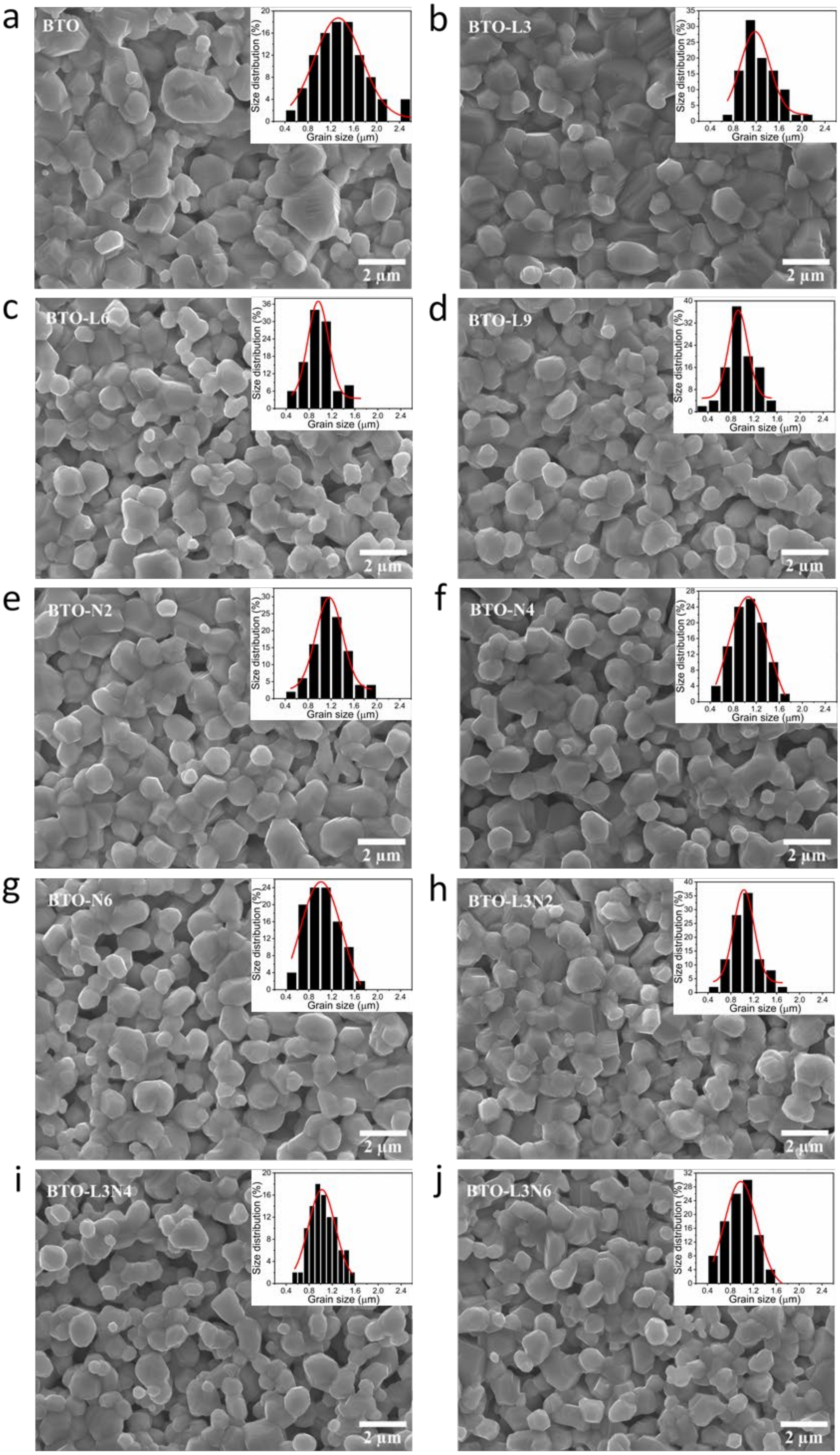

Fig. S2 SEM images of a. BTO, b. BTO-L3, c. BTO-L6, d. BTO-L9, e. BTO-N2, f. BTO-N4, g. BTO-N6, h. BTO-L3N2, i. BTO-L3N4, j. BTO-L3N6 samples (sample labels explained in Table 1); inserted patterns to show the grains sizes of the samples determined using ImageJ software, and the size distributions analysed with a Gaussian function.

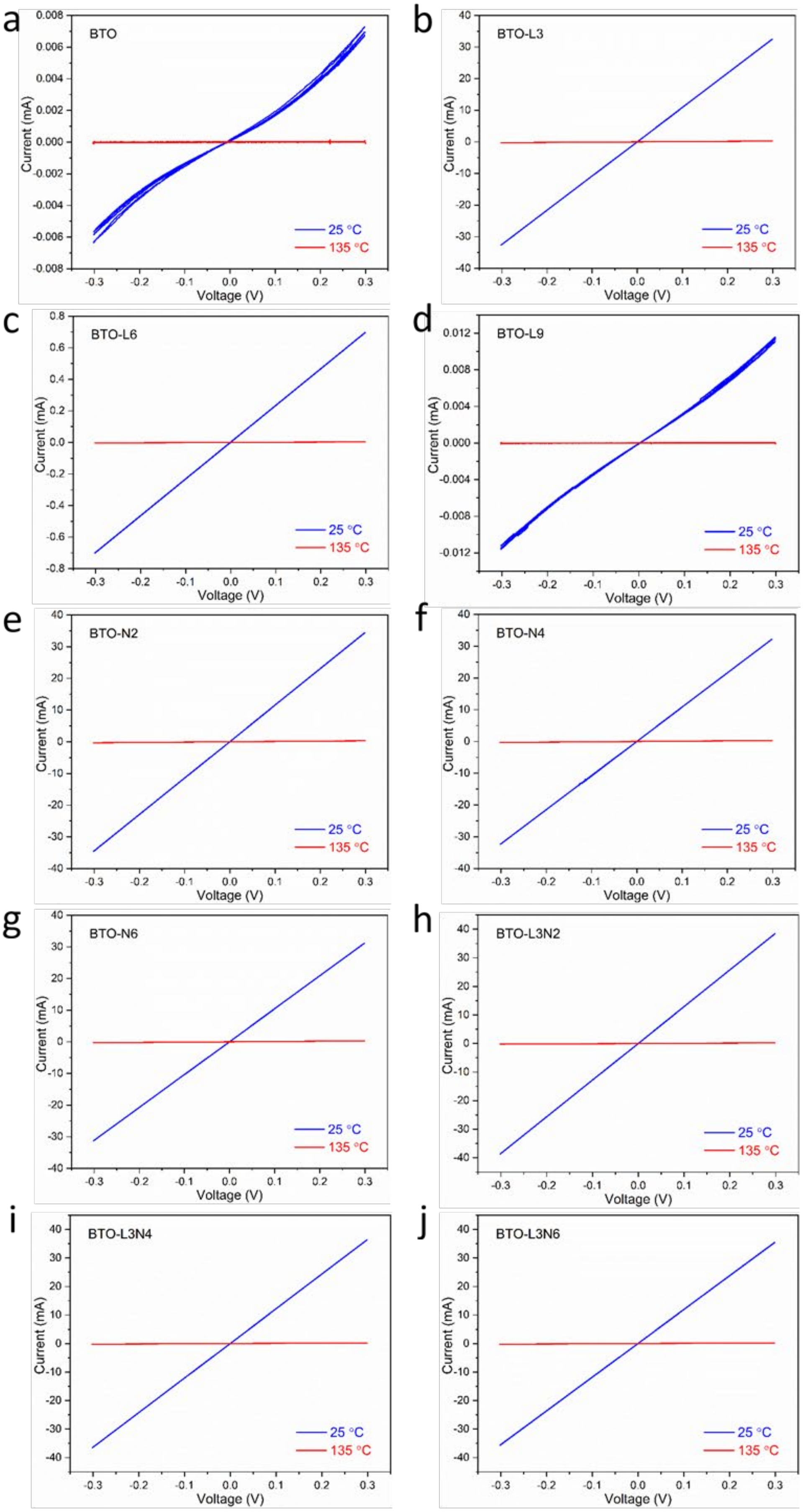

Fig. S3 Current-voltage plots (3 cycles each) for a. BTO, b. BTO-L3, c. BTO-L6, d. BTO-L9, e. BTO-N2, f. BTO-N4, g. BTO-N6, h. BTO-L3N2, i. BTO-L3N4, j. BTO-L3N6 samples, cycling at scanning rate of 20 mV s^{-1}, showing the ohmic behaviour of the samples (sample labels explained in Table 1).

Estimation of ohmic voltage drops produced by the La and Nb co-doped $BaTiO_3$ PTCR film in batteries:

The optimised solid-state synthesis procedure of La and Nb co-doped $BaTiO_3$ produces films of ca. 200 µm thickness, room temperature conductivity of 2.71×10^{-3} S cm^{-1} and high temperature conductivity of 1.58×10^{-5} S cm^{-1}. With this, the area-normalised resistance of the film can be obtained as:

0.02 cm / 2.71×10^{-3} S cm^{-1} ≈ 7.38 Ω cm^{2} at room temperature

0.02 cm / 1.58×10^{-5} S cm^{-1} ≈ 1266 Ω cm^{2} at high temperature (135 °C)

For the estimation of the effect of the PTCR film in practical batteries, we will consider an example of a practical battery of areal capacity of 2 mA h cm^{-2} operated at a current rate of 1C, and hence with an area-normalised current of 2 mA cm^{-2}. The ohmic drop produced by the PTCR film at that current is obtained as follows:

0.002 A cm^{-2} $\times$ 7.38 Ω cm^{2} ≈ 0.015 V at room temperature

0.002 A cm^{-2} $\times$ 1266 Ω cm^{2} ≈ 2.5 V at high temperature (135 °C)

The above calculations show that a dramatic ohmic voltage drop occurs at the PTCR film at high temperature for the current densities typically employed in lithium-ion batteries. Consequently, at high temperature, a commercial battery incorporating a PTCR film would quickly reach the pre-set voltage limits of operation, and thus electrochemical reactions would become very slow. On the contrary, the ohmic voltage drop at room temperature is only moderate, and thus the battery would be able to operate normally in the presence of the PTCR film.

For the experiments presented in this article, the $LiFePO_4$ electrode loading is ca. 12 mg cm^{-2} and, thus, a specific current of 17 mA g^{-1} for C/10 experiments corresponds to an area-normalised current of 0.204 mA cm^{-2}. The associated ohmic drops produced at the PTCR film are obtained as follows:

0.204×10^{-3} A cm^{-2} $\times$ 7.38 Ω cm^{2} ≈ 0.0015 V at room temperature

0.204×10^{-3} A cm^{-2} $\times$ 1266 Ω cm^{2} ≈ 0.25 V at high temperature (135 °C)

The above calculations show that, for the La and Nb co-doped $BaTiO_3$ film, the combination of sufficiently high room temperature conductivity and sufficiently low film thickness, produces negligible ohmic drop in batteries at room temperature, which explains why the battery can work in the presence of the PTCR film. Although these estimations produce a moderate voltage drop at high temperature, in practice, it is observed that the presence of the PTCR film effectively suppressed the capacity of $LiFePO_4$ cells at high temperature (see Fig. 4c).

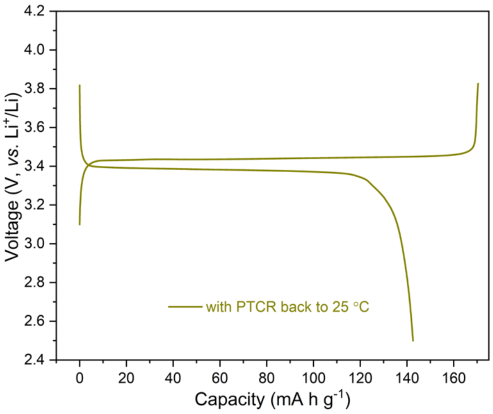

Fig. S4 0.1C galvanostatic charge/discharge plot of lithium-ion battery with the PTCR film when the temperature was set back to 25 °C, after the thermal treatment at 135 °C shown in Fig. 4c.

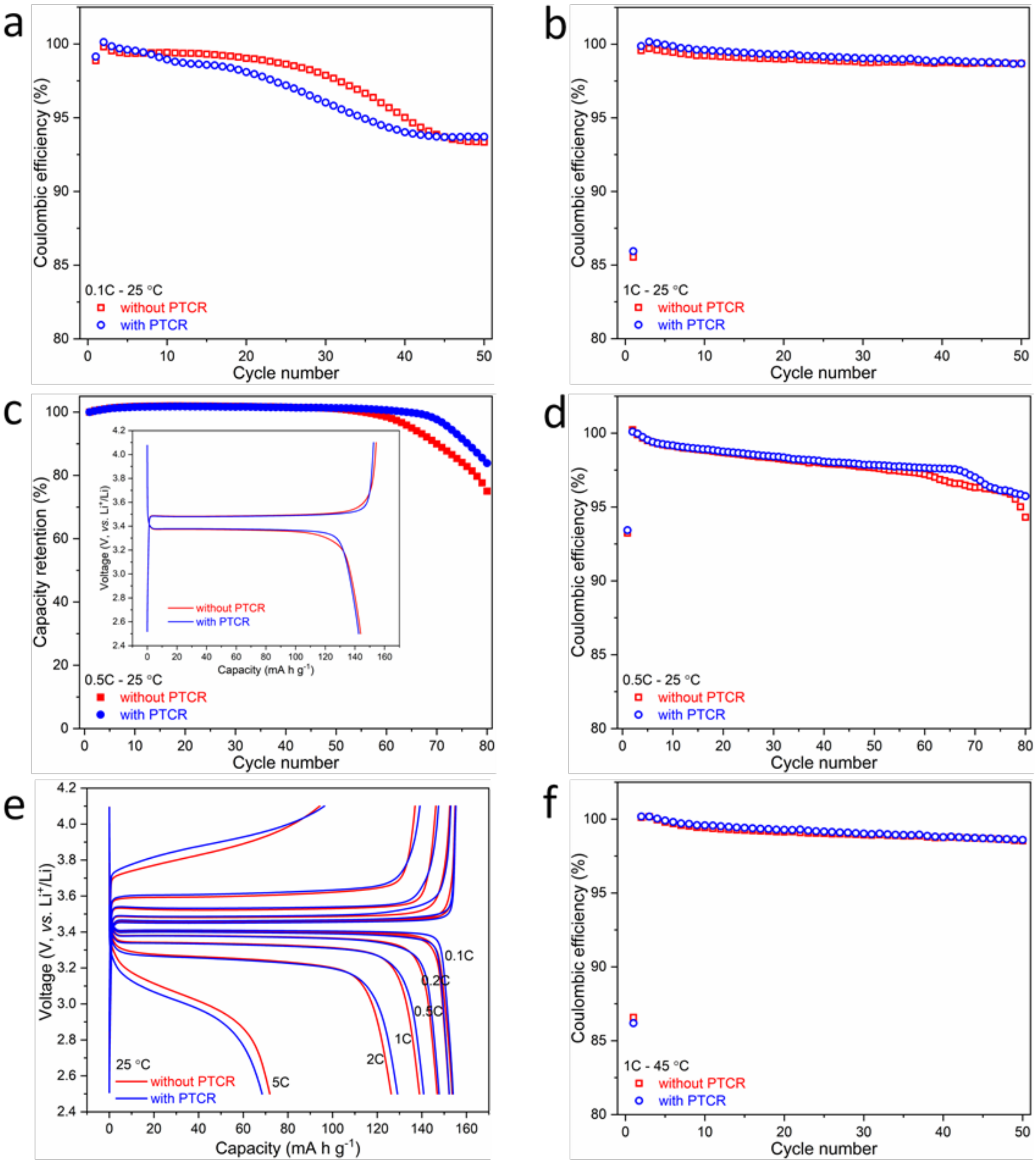

Fig. S5 Electrochemical performances of $LiFePO_4$ half cells with and without the PTCR film: Coulombic efficiency *vs.* cycle number at a current rate of a. 0.1C and b. 1C at 25 °C; c. galvanostatic cycling performances and charge/discharge plots (inset) at a current rate of 0.5C at 25 °C; d. Coulombic efficiency *vs.* cycle number at a current rate of 0.5C at 25 °C; e. the charge/discharge plots at various sequential rates from 0.1C to 5C at 25 °C; f. Coulombic efficiency *vs*. cycle number at a current rate of 1C at 45 °C.

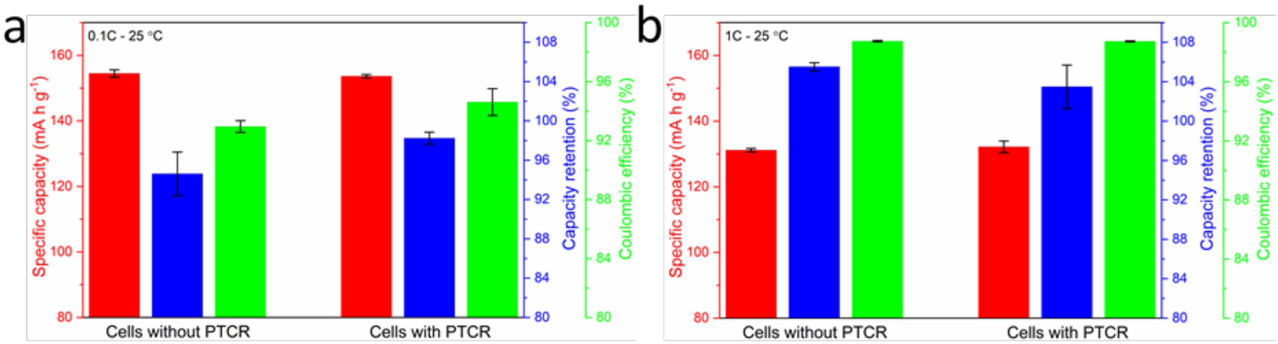

Fig. S6 Comparison of electrochemical performances of $LiFePO_4$ half cells with and without the PTCR film: the specific discharge capacities in the initial cycle, capacity retentions and Coulombic efficiencies after 50 cycles at a current rate of a. 0.1C and b. 1C at 25 °C. Error bars show the differences in repeat experiments.

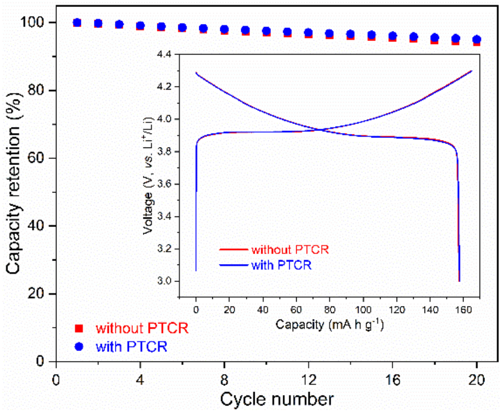

Fig. S7 Electrochemical performances of $LiCoO_2$ half cells with and without the PTCR film: galvanostatic cycling performances and charge/discharge plots (inset) at a current rate of 0.1C at 25 °C.

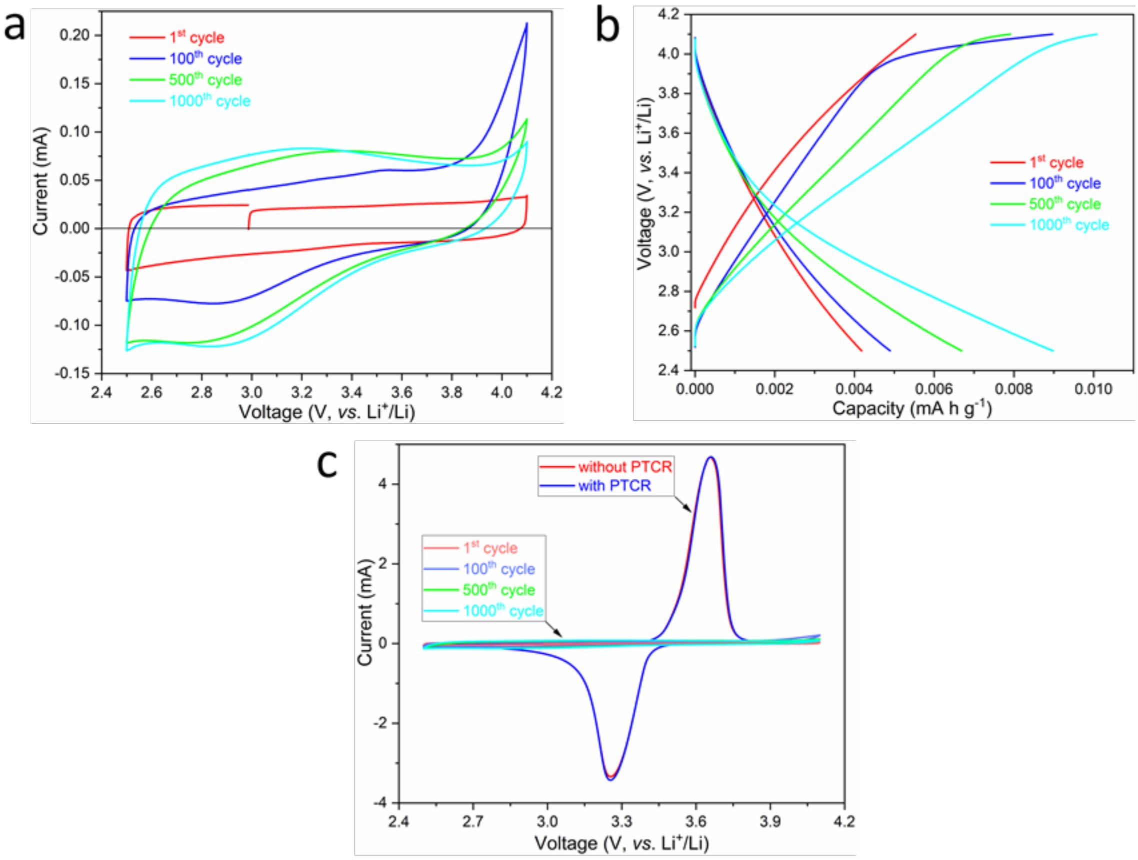

Fig. S8 a. Cyclic voltammetry plots of battery with the $BaTiO_3$-based PTCR film as cathode and Li as anode at 20 mV s^{-1} over the range of 2.5 to 4.1 V for 1000 cycles; b. charge/discharge plots of battery with PTCR film as cathode and Li as anode under galvanostatic cycling between 2.5 and 4.1 V for 1000 cycles. c. comparison of the cyclic voltammograms measured with the $BaTiO_3$-based PTCR film in a and the cyclic voltammograms measured with $LiFePO_4$ cathodes in Fig. 4a.

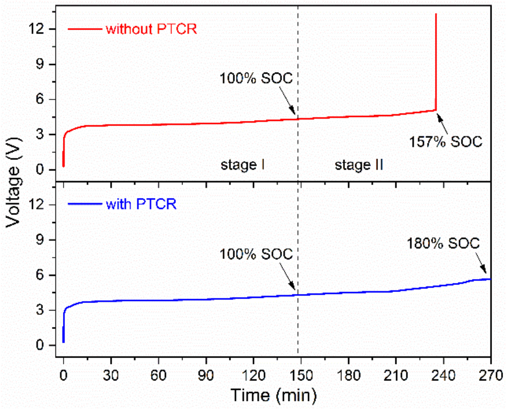

Fig. S9 Voltage changes during overcharging tests for $LiCoO_2$-graphite cells with and without the BTO-L3N2 PTCR film.

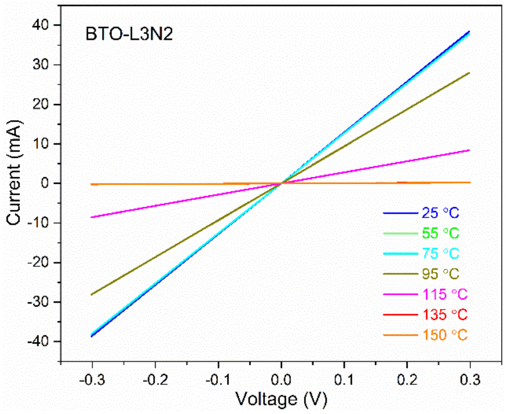

Fig. S10 Current-voltage plots (3 cycles each) for BTO-L3N2 sample at different temperatures from 25 to 150 °C, cycling at scanning rate of 20 mV s^{-1}, showing the ohmic behaviour of the sample (sample label explained in Table 1). Note that the blue and green lines are coincident with the cyan line, and the red line is coincident with the orange line.

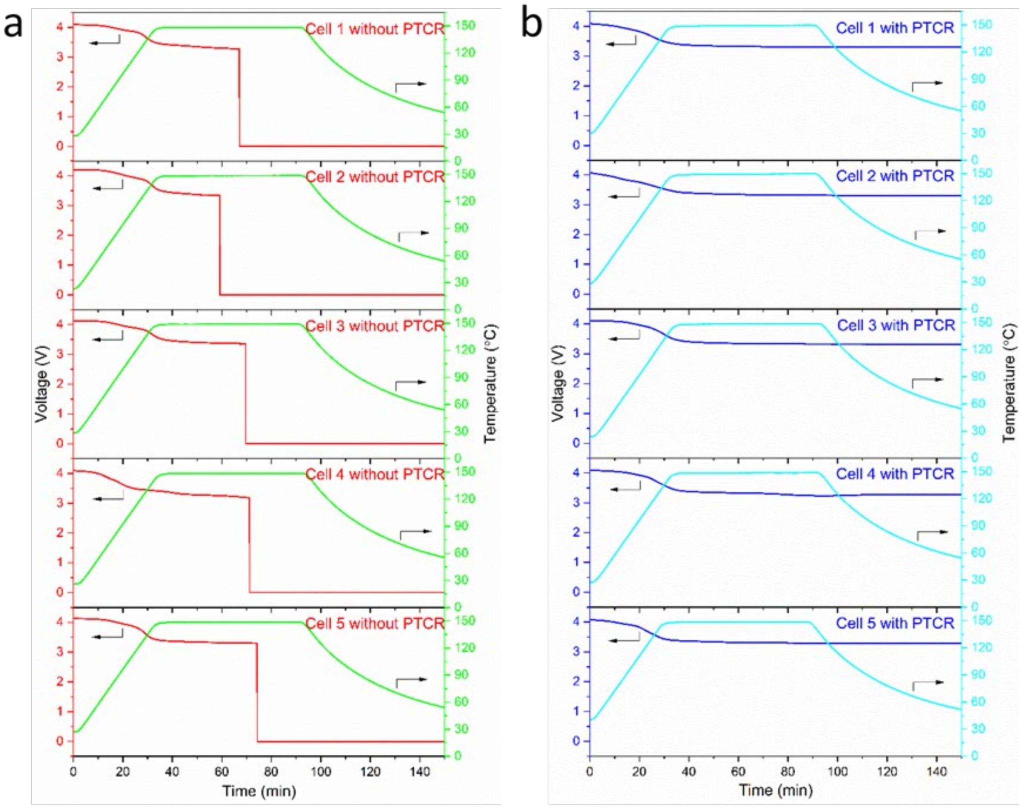

Fig. S11 Voltage and skin temperature changes during heating tests at 150 °C for $LiFePO_4$-graphite full cells a. without and b. with the BTO-L3N2 PTCR film.

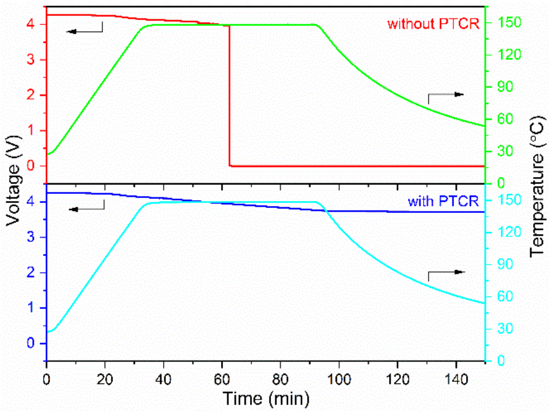

Fig. S12 Voltage and temperature changes during heating tests at 150 °C for $LiCoO_2$-graphite cells with and without the BTO-L3N2 PTCR film.

References

1. S.-S. Ryu, H.-T. Kim, H. J. Kim and S. Kim, *J. Ceram. Soc. Jpn.*, 2009, **117**, 811-814.
2. P. Ctibor, H. Ageorges, J. Sedlacek and R. Ctvrtlik, *Ceram. Int.*, 2010, **36**, 2155-2162.
3. Q. D. Nguyen, E.-S. Oh and K.-H. Chung, *Polym. Test.*, 2019, **76**, 245-253.
4. G. Y. Gor, J. Cannarella, C. Z. Leng, A. Vishnyakov and C. B. Arnold, *J. Power Sources*, 2015, **294**, 167-172.
5. H. Y. Sun, Y. Takeda, N. Imanishi, O. Yamamoto and H.-J. Sohn, *J. Electrochem. Soc.*, 2000, **147**, 2462-2467.
6. M. Acosta, R. Detsch, A. Grünewald, V. Rojas, J. Schultheiß, A. Wajda, R. W. Stark, S. Narayan, M. Sitarz, J. Koruza and A. R. Boccaccini, *J. Am. Ceram. Soc.*, 2018, **101**, 440-449.
7. G. Wypych, *Handbook of Fillers*, ChemTec Publishing, 2016.
8. M. Wang, Q. Tan, L. Liu and J. Li, *ACS Sustain. Chem. Eng.*, 2019, **7**, 12799-12806.
9. J. Michal, J. Mitera and S. Tardon, *Fire Mater.*, 1976, **1**, 160-168.